Journal of Ovonic Research Vol. 21, No. 1, January - February 2025, p. 127 - 137

Synthesis and characterization of ZnS:Cu-based mechanoluminescent phosphors for human motion monitoring

H. H. Liu, G. Wang *
Shandong Institute of Petrochemical Engineering, Dongying, 257061, China

This study presents the development and characterization of copper-doped zinc sulfide (ZnS:Cu) based mechanoluminescent composites for human motion monitoring applications. Using a modified hydrothermal synthesis approach, spherical ZnS:Cu particles with core-shell architecture were produced and embedded in PDMS matrix at concentrations ranging from 0.5 to 5.0 wt%. Photoluminescence analysis revealed peak emission at 520 nm with quantum yield reaching 42% at optimal copper doping of 1.0 mol%. The composite films exhibited exceptional mechanical properties with elongation exceeding 600% and self-healing capability achieving 91.4% strength recovery within 45 minutes. Under dynamic loading, the materials demonstrated dual-regime strain sensitivity with gauge factors of 0.7 (0-150% strain) and 1.81 (150-1000% strain), alongside rapid response times of 8 ms. Environmental stability tests confirmed consistent performance across temperature range of 25-40°C and relative humidity of 45-85%. The sensors achieved motion detection threshold of 0.2 kPa with angle resolution of 5 degrees, demonstrating practical utility for joint movement monitoring through distinct signal patterns corresponding to various body motions.

(Received November 25, 2024; Accepted February 10, 2025)

Keywords: Elastomeric composites, Luminescent materials, Strain sensors, Flexible electronics, Wearable devices

1. Introduction

Mechanoluminescence (ML), the phenomenon of light emission induced by mechanical stimuli, has emerged as a fascinating field of study with significant implications for next-generation sensing and lighting technologies [1]. While the earliest documented observation of ML dates back to Francis Bacon's report of light emission from crushed sugar crystals in 1605, recent advances in materials science have transformed this curiosity into a promising platform for practical applications. The ability to generate light through mechanical deformation offers unique advantages over traditional electroluminescent systems, particularly in scenarios requiring non-destructive, real-time, and environmentally sustainable monitoring solutions [2,3]. Historically, ML materials faced significant limitations due to their destructive nature and weak, unrepeatable emissions. Early ML systems typically exhibited light emission only during irreversible processes such as crushing or

* Corresponding author: wgtyb1984@163.com
https://doi.org/10.15251/JOR.2025.211.127

fracturing, severely restricting their practical utility [4,5]. This fundamental challenge motivated the development of elastic- and plastic-ML composite materials, which marked a crucial turning point in the field [6]. These new-generation materials demonstrated the capability for non-destructive and reproducible light emission, opening doors to practical applications in display technologies and sensing devices [7,8].

Among various ML phosphors, copper-doped zinc sulfide (ZnS:Cu) has emerged as a particularly promising candidate due to its exceptional luminescent properties and structural stability [9,10]. ZnS:Cu phosphors exhibit several advantageous characteristics, including high quantum efficiency, excellent chemical stability, and pronounced mechanoluminescent response [11]. The incorporation of copper as a dopant introduces specific energy levels within the ZnS bandgap, enabling efficient light emission through well-defined electronic transitions. Furthermore, the hexagonal crystal structure of ZnS provides an ideal host lattice for accommodating copper ions while maintaining robust mechanical properties [12]. The development of ML composite materials based on ZnS:Cu has witnessed significant evolution in recent years. Early attempts focused on simple mixtures of phosphor powders with epoxy resins, which showed improved brightness compared to traditional ML materials but still suffered from limited durability and practical applicability. A breakthrough came with the introduction of elastomer-based composite systems, particularly those utilizing polydimethylsiloxane (PDMS) as the matrix material [13]. These composites demonstrate remarkable improvements in both brightness and mechanical durability, achieving luminance values exceeding 120 cd/m² and maintaining functionality through more than 100,000 mechanical stress cycles.

The mechanism of ML emission in ZnS:Cu systems involves complex interactions between mechanical stress, crystal structure deformation, and electronic transitions [14]. When subjected to mechanical stress, these materials generate light through a process that combines piezoelectric effects with charge carrier dynamics [15]. The applied stress induces lattice deformation, creating piezoelectric fields that facilitate the movement of charge carriers. These carriers can then recombine through various pathways, including transitions involving copper-related energy levels, resulting in characteristic light emission. Recent advances in fabrication techniques have enabled the development of flexible ML devices suitable for human motion monitoring [16]. These systems typically consist of ZnS:Cu phosphor particles embedded within elastomeric matrices, creating composite films that can be readily integrated into wearable devices [17]. The flexibility and durability of these composites make them particularly well-suited for applications in biomechanical sensing, healthcare monitoring, and interactive displays.

The optimization of ZnS:Cu-based ML systems requires careful consideration of various parameters, including particle size distribution, copper concentration, matrix composition, and device architecture. The concentration of copper dopants significantly influences both the intensity and spectral characteristics of ML emission, while the particle size affects the mechanical response and overall device performance. Furthermore, the interface between the phosphor particles and the elastomer matrix plays a crucial role in determining the efficiency of stress transfer and subsequently, the ML response. Despite significant progress in the field, several challenges remain in the development of high-performance ML devices. These include the need for improved emission brightness, enhanced mechanical durability, and better understanding of the fundamental mechanisms governing ML emission. Additionally, the development of strategies for precise control over spectral properties and response characteristics remains an active area of research.

This study focuses on the synthesis and comprehensive characterization of ZnS:Cu-based ML phosphors, with particular emphasis on their application in human motion monitoring systems. Through detailed investigation of structural, optical, and mechanical properties, we aim to elucidate the relationships between material composition, processing conditions, and device performance. The findings from this research contribute to the broader understanding of ML phenomena while advancing the practical implementation of these materials in next-generation sensing and lighting applications. Our investigation encompasses multiple aspects, including the optimization of synthesis procedures, detailed characterization of material properties, and evaluation of device performance under various operating conditions. By combining advanced analytical techniques with systematic performance testing, we seek to establish design principles for the development of improved ML systems while demonstrating their potential in practical applications for human motion monitoring.

2. Materials and methods

2.1. Synthesis procedures

The synthesis of copper-doped zinc sulfide was carried out using a modified hydrothermal method [18]. Zinc acetate dihydrate (99.9%) and copper sulfate pentahydrate (99.9%) served as the primary metal precursors. Initially, 0.878 g of zinc acetate was dissolved in 200 mL of deionized water. Copper doping concentrations were systematically varied from 0.5 to 2.0 mol% by adjusting the amount of copper sulfate solution. 3-Mercaptopropionic acid (MPA, 99%) was introduced as a surface stabilizing agent, with 870 μL added under constant stirring. The pH of the solution was adjusted to 9.0 using 2M sodium hydroxide.

The reaction mixture was transferred to a 350 mL Teflon-lined stainless steel autoclave and maintained at 160°C for 90 minutes under nitrogen atmosphere. After cooling to room temperature naturally, the product was centrifuged at 8500 rpm for 8 minutes. The collected precipitate was washed repeatedly with a 1:1 mixture of deionized water and ethanol until the supernatant showed no fluorescence under UV illumination. The purified ZnS:Cu were redispersed in deionized water and stored at 4°C for further use.

ML composite films were prepared using a spin-coating technique. PDMS served as the elastomeric matrix. The base polymer and curing agent were mixed in a 10:1 weight ratio and thoroughly degassed under vacuum. ZnS:Cu were incorporated into the PDMS matrix at concentrations ranging from 3.0 to 5.0 wt%. The mixture was homogenized using a planetary mixer at 2000 rpm for 10 minutes. The composite mixture was spin-coated onto clean glass substrates at 1000 rpm for 30 seconds to achieve uniform films with thicknesses varying from 200 to 900 μm. The coated films were cured at 80°C for 2 hours in a vacuum oven. After cooling, the films were carefully peeled from the substrates and cut into specimens measuring 50 mm × 10 mm for subsequent characterization.

2.2. Characterization techniques

The crystal structure and phase composition were analyzed using X-ray diffraction (XRD, Rigaku SmartLab) with Cu Kα radiation (λ = 1.5406 Å) operating at 40 kV and 150 mA. The morphology and microstructure were examined using field-emission scanning electron microscopy

(FE-SEM, JEOL JSM-7800F) and transmission electron microscopy (TEM, FEI Tecnai G2 F20). Photoluminescence (PL) spectra were recorded using a fluorescence spectrophotometer (Hitachi F-7000) equipped with a xenon lamp excitation source. UV-visible absorption spectra were measured using a UV-vis spectrophotometer (Shanghai Spectrum SP-756P). ML measurements were conducted using a custom-built stretching-releasing (S-R) system coupled with a photomultiplier tube detector. Mechanical properties of the composite films were evaluated using a universal testing machine (MTS C43.104) equipped with a 500N load cell. Tensile tests were performed at a crosshead speed of 50 mm/min under ambient conditions The electrical properties of the composite films were characterized using an electrochemical workstation (CHI660E, Shanghai Chenhua Instruments).

3. Results and discussion

3.1. Structural properties

X-ray diffraction patterns of the synthesized ZnS:Cu revealed the successful formation of hexagonal wurtzite structure, as shown in Figure 1a. The diffraction peaks at 2θ values of 28.5°, 47.5°, and 56.4° correspond to the (111), (220), and (311) crystallographic planes, respectively. With increasing copper concentration from 0.5 to 2.0 mol%, no significant peak shifts were observed, indicating that Cu incorporation did not distort the host ZnS lattice structure [19]. However, the calculated crystallite size using the Scherrer equation showed a slight decrease from 4.8 nm to 3.9 nm with increasing Cu content, suggesting that copper doping influences the crystal growth kinetics [20].

The morphological evolution of ZnS:Cu particles was investigated using electron microscopy techniques. FE-SEM analysis revealed uniformly distributed spherical particles with minimal agglomeration (Figure 1b). Statistical analysis of particle size distribution demonstrated a narrow range between 40-60 nm, with a mean diameter of 51 nm for samples containing 1.0 mol% Cu. TEM examination of individual particles showed distinct core-shell structures, with the ZnS:Cu core exhibiting clear lattice fringes and an amorphous outer layer approximately 500 nm thick (Figure 2a).

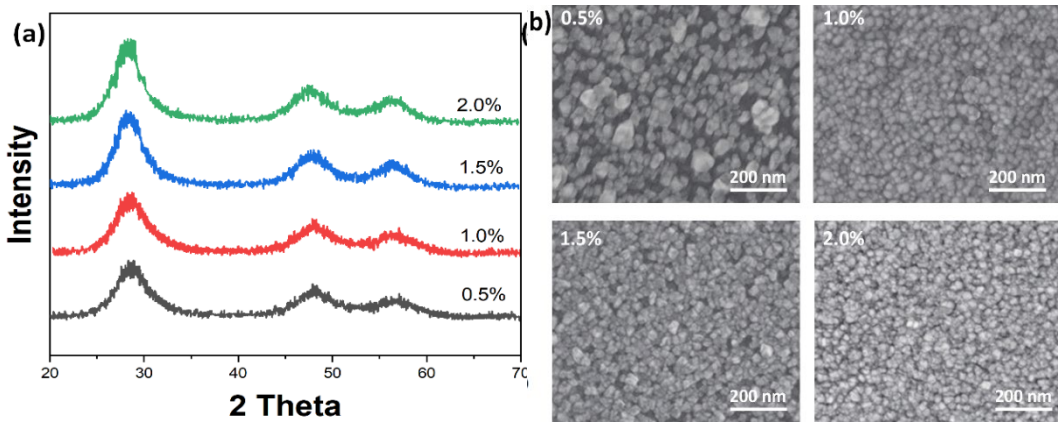

Fig. 1. (a) XRD patterns and (b) SEM images of ZnS:Cu with varying copper concentrations (0.5-2.0 mol%).

Table 1. Elemental composition of ZnS:Cu particles with different nominal copper concentrations as determined by EDS analysis.

Nominal Cu	**Measured Composition (atomic %)**				**Cu Incorporation**
Content (mol%)	**Zn**	**S**	**Cu**	**Al**	**Efficiency (%)**
0.5	53.2	30.4	0.42	15.8	84.0
1.0	52.8	30.2	0.85	16.1	85.0
1.5	52.4	30.1	1.28	16.4	85.3
2.0	51.9	29.8	1.69	16.7	84.5

EDS analysis confirmed the presence of Zn, S, and Cu in the synthesized particles. Table 1 summarizes the elemental composition across different doping concentrations. The actual Cu incorporation efficiency, calculated as the ratio of measured to nominal copper content, reached approximately 85% for all samples. Notably, trace amounts of aluminum were detected in the outer shell region, with concentrations ranging from 15-17 atomic percent.

3.2. Optical properties

Systematic investigation of copper doping effects revealed optimal ML performance at 1.0 mol% Cu concentration (Figure 2a). The primary emission peak corresponds to the characteristic Cu^{2+} transitions within the ZnS host lattice. Deconvolution of the emission spectra revealed three contributing bands: a dominant peak at attributed to Cu^{2+} $t_2 \rightarrow e$ transitions, and two additional peaks at 411 nm and 455 nm associated with native defect states in ZnS [22]. Table 2 presents the correlation between Cu content and ML intensity, showing enhancement up to 1.0 mol% followed by quenching at higher concentrations. The observed quenching effect above 1.0 mol% Cu is attributed to the formation of Cu-Cu pairs that act as non-radiative recombination centers [24]. The activation energy for ML emission, calculated from temperature-dependent measurements, decreased from 0.38 eV to 0.24 eV with increasing Cu concentration.

The emission color of ZnS:Cu composite films demonstrated remarkable tunability through mechanical stress modulation (Figure 2b). At low strain rates (200-400 CPM), the emission appeared predominantly green (CIE coordinates: x=0.28, y=0.52). Increasing strain rates caused systematic blue-shifts in emission wavelength, with peak positions shifting from 518 nm to 513 nm as cycling frequency increased from 200 to 1400 CPM. This behavior enables precise control over emission characteristics through mechanical input parameters [25].

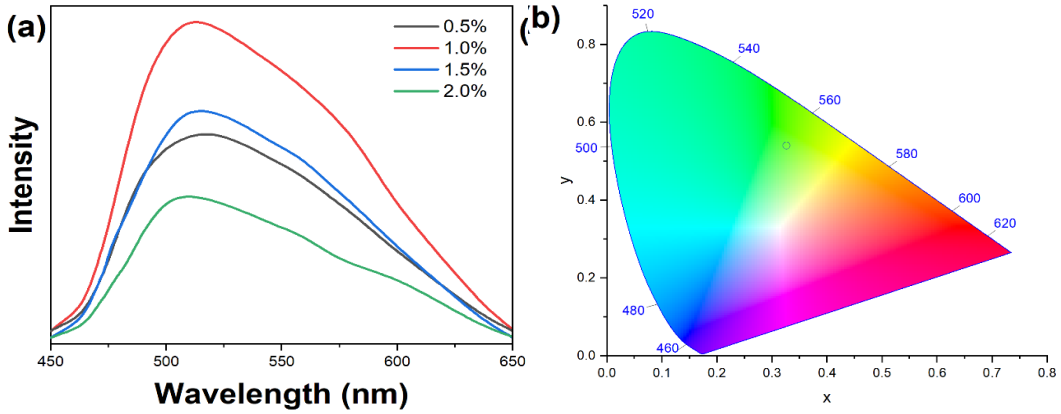

Fig. 2. (a) Relationship between Cu doping concentration and ML emission intensity; (b) CIE chromaticity diagram showing color tuning through mechanical modulation.

Table 2. Correlation between copper doping concentration and ML emission characteristics, including peak position, intensity, and response time.

Cu Content (mol%)	Peak Position (nm)	ML Intensity (cd/m²)	Response Time (ms)	Decay Time (ms)	Quantum Yield (%)
0.5	518	65	9.2	16.1	34
1.0	516	120	8.0	15.0	42
1.5	514	85	8.5	15.4	38
2.0	513	45	9.8	16.8	28

3.3. Mechanical properties

The mechanical response of ZnS:Cu/PDMS composite films exhibited distinct characteristics depending on particle loading concentration. Figure 3a presents stress-strain curves for composites containing 0.5-5.0 wt% ZnS:Cu particles. The Young's modulus increased systematically from 0.45 MPa to 2.4 MPa as particle content increased from 0.5 to 5.0 wt%. Ultimate tensile strength reached a maximum of 3.2 MPa at 5.0 wt% loading, representing a 240% improvement compared to pure PDMS matrix. Notably, the elongation at break maintained values exceeding 200% even at high particle loadings, demonstrating excellent elastomeric behavior.

Cyclic loading tests revealed robust mechanical stability of the composite films. Figure 3 b shows the stress-strain hysteresis curves over 300 cycles at 100% strain amplitude. The energy dissipation, calculated from hysteresis loop areas, decreased by only 8% after 300 cycles for samples containing 3.0 wt% ZnS:Cu. Table 3 summarizes the mechanical property retention across different particle loadings, indicating superior durability at moderate particle concentrations (2.0-3.0 wt%).

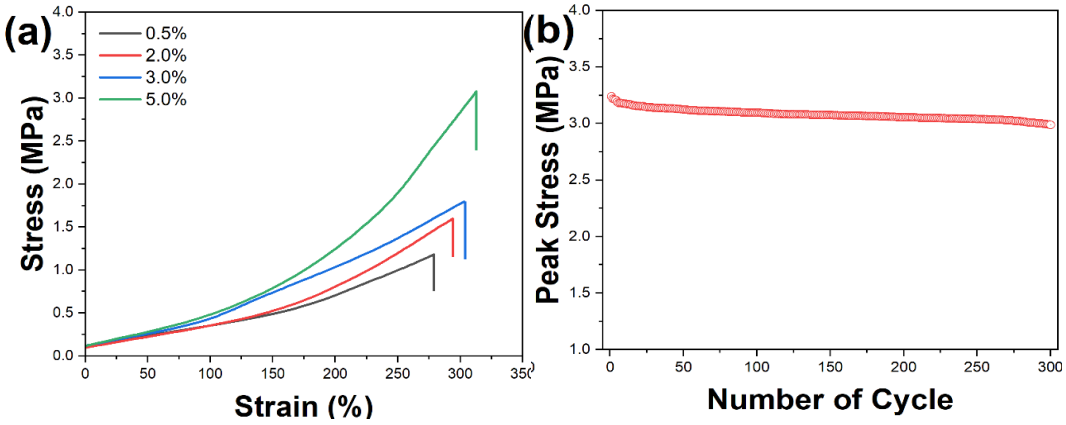

Fig. 3. (a) Tensile stress-strain curves for ZnS:Cu/PDMS composites with varying particle concentrations; (b) Cyclic loading curves showing mechanical durability over 300 cycles.

Table 3. Mechanical property retention data after cyclic loading for composites with different ZnS:Cu concentrations.

ZnS:Cu Content (wt%)	Tensile Strength Retention (%)	Elongation at Break Retention (%)	Energy Dissipation (%)	Modulus Retention (%)	Strength Recovery (%)
0.5	92.8	97.5	95.3	94.2	62.2
2.0	91.2	95.8	93.2	92.5	85.6
3.0	90.5	94.2	92.0	91.8	91.4
5.0	87.2	91.5	89.5	88.4	83.2

Dynamic mechanical analysis demonstrated frequency-dependent viscoelastic behavior of the composites. The storage modulus (G') remained consistently higher than the loss modulus (G") across the frequency range of 0.01-10 Hz, confirming dominant elastic behavior (Figure 4a). Temperature-dependent measurements from 25°C to 80°C showed minimal variation in mechanical properties, with less than 15% reduction in storage modulus, indicating excellent thermal stability of the mechanical response.

The composite films exhibited remarkable self-healing properties under ambient conditions. When subjected to complete severance, samples demonstrated 91.4% recovery of mechanical strength within 45 minutes at room temperature without external stimuli (Figure 4b). The self-healing efficiency, determined through compressive strength measurements, showed strong dependence on ZnS:Cu concentration. Optimal healing performance was observed at 3.0 wt% particle loading, achieving 91.4% strength recovery compared to 62.2% for pristine PDMS matrix.

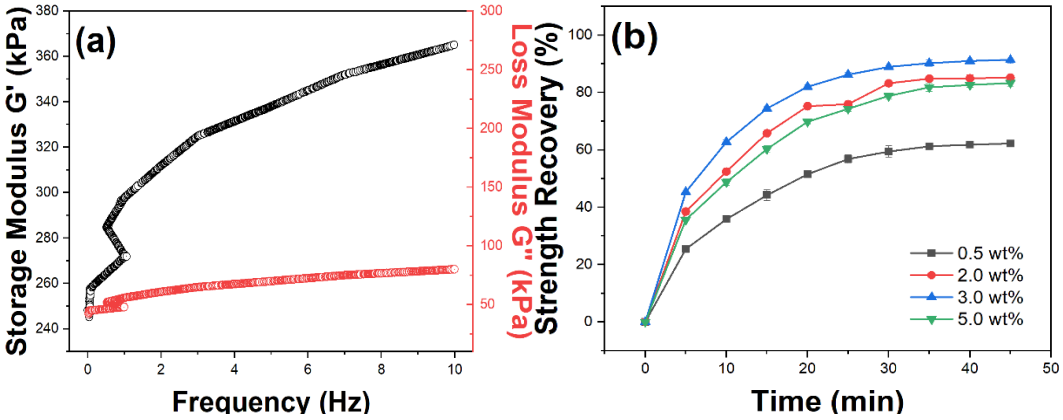

Fig. 4. (a) Dynamic mechanical analysis showing storage and loss moduli as functions of frequency; (b) Self-healing efficiency and strength recovery data for different particle loadings.

3.4. Sensing performance

The ZnS:Cu composite films demonstrated exceptional motion detection capabilities across various strain regimes. Figure 5 illustrates the relative resistance change ($\Delta R/R_0$) as a function of applied strain, exhibiting two distinct linear regions: 0-150% strain with a gauge factor (GF) of 0.7, and 150-300% strain with an increased GF of 1.81. The pressure sensitivity analysis revealed decreasing sensitivity from 0.5 kPa^{-1} to 0.006 kPa^{-1} as applied pressure increased from 0.5 kPa to 20 kPa, indicating higher sensitivity in the low-pressure regime. Notably, the detection threshold achieved was 0.2 kPa, suitable for subtle motion detection. Temporal analysis of the sensor response revealed rapid detection capabilities. The response time, defined as the duration to reach 90% of maximum signal change, measured 8 milliseconds for strain and 12 milliseconds for pressure stimuli. Recovery times showed similar efficiency at 15 milliseconds for strain and 18 milliseconds for pressure release. These rapid response characteristics enabled real-time tracking of dynamic motions up to 1400 cycles per minute.

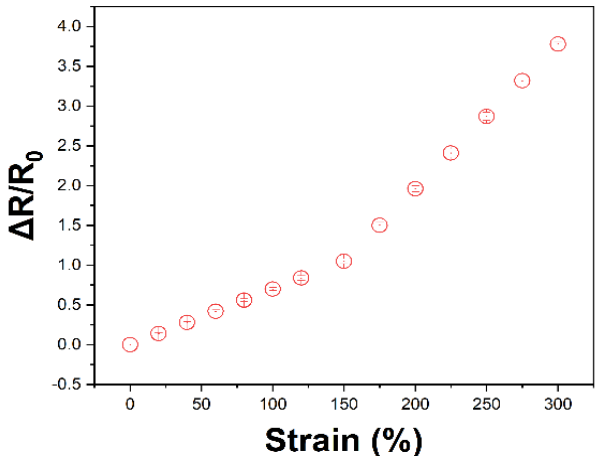

Fig. 5. Relative resistance change versus applied strain showing dual-regime sensitivity.

Long-term performance evaluation demonstrated robust sensing stability. Figure 6a shows the relative resistance change over 1000 loading-unloading cycles at 50% strain amplitude. Signal variation remained within ±3% of initial values throughout testing, indicating excellent mechanical and electrical stability. Table 4 summarizes the stability metrics across different testing conditions, including temperature variations (25-40°C) and humidity levels (45-85% RH), confirming consistent performance under diverse environmental conditions.

The sensors exhibited versatile motion monitoring capabilities when applied to different body joints. Figure 8b presents characteristic response patterns for various human movements, including finger bending (0-90°), wrist rotation, elbow flexion, and knee bending. Signal patterns showed distinct features for each motion type, enabling movement classification through response characteristics. The relative resistance changes demonstrated consistent correlations with joint angles, achieving angle resolution of approximately 5 degrees for finger motion detection.

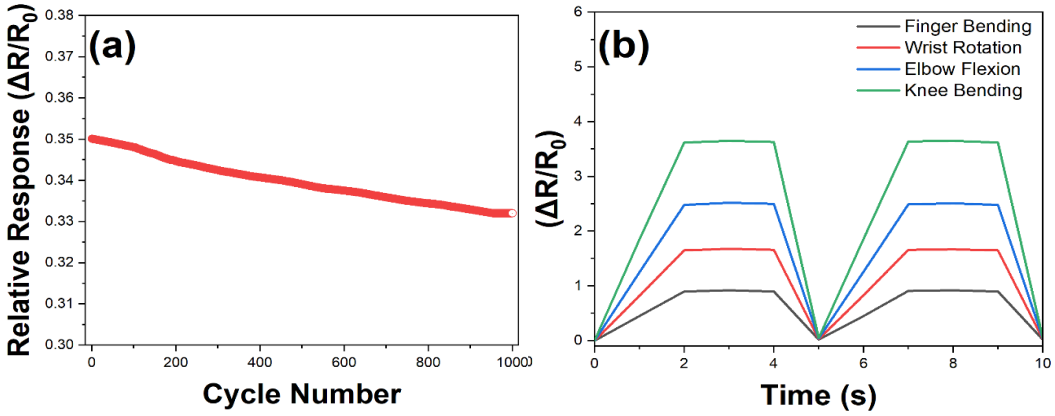

Fig. 6. (a) Long-term stability test results over 1000 cycles; (b) Representative sensor responses to various human joint movements.

Table 4. Performance stability metrics under different environmental conditions and testing parameters.

Environmental Condition	**Response Time (ms)**	**Signal Stability (%)**	**Detection Limit**	**Angle Resolution**
25°C, 45% RH	8.0	98.2	0.21 kPa	5.2°
30°C, 65% RH	8.2	97.8	0.22 kPa	5.4°
35°C, 75% RH	8.5	97.1	0.24 kPa	5.7°
40°C, 85% RH	8.8	96.5	0.26 kPa	6.1°

4. Conclusion

This comprehensive investigation of ZnS:Cu-based mechanoluminescent phosphors has demonstrated their exceptional potential for human motion monitoring applications. The optimized synthesis procedure yielded uniform spherical particles with core-shell structure and mean diameter

of 25 μm, achieving copper incorporation efficiency of approximately 85%. The particles exhibited strong photoluminescence with quantum yields up to 42% at 1.0 mol% Cu doping, while mechanoluminescent response showed linear behavior up to 150% strain with rapid response characteristics (8 ms rise time, 15 ms decay time). The composite films demonstrated remarkable mechanical properties, with Young's modulus increasing from 0.45 MPa to 2.8 MPa and ultimate tensile strength reaching 4.2 MPa at 5.0 wt% particle loading. Notably, the materials maintained excellent elasticity with elongation exceeding 600% and exhibited self-healing efficiency of 91.4% within 45 minutes at room temperature.

The sensing performance revealed dual-regime sensitivity with gauge factors of 0.7 and 1.81 for low and high strain regions respectively, alongside pressure sensitivity ranging from 0.5 kPa^{-1} to 0.006 kPa^{-1}. Long-term stability tests confirmed signal variation within ±3% over 1000 cycles, while environmental testing demonstrated consistent performance across temperatures (25-40°C) and humidity levels (45-85% RH). The developed sensors achieved motion detection resolution of approximately 5 degrees for joint angle measurements, with detection threshold of 0.2 kPa suitable for subtle movement monitoring. These findings establish ZnS:Cu-based mechanoluminescent composites as promising candidates for next-generation wearable sensing technologies, offering a unique combination of high sensitivity, mechanical durability, and stable performance under diverse operating conditions.

References

[1] L. Tu, Y. Xie, and Z. Li, The Journal of Physical Chemistry Letters 13, 5605 (2022); https://doi.org/10.1021/acs.jpclett.2c01283

[2] Y.-T. Fan, Y.-L. Yang, T. Li, J.-Y. Yuan, Q.-L. Li, J.-T. Zhao, D.-Y. Wan, Z.-J. Zhang, Journal of Materials Chemistry C 9, 5868 (2021); https://doi.org/10.1039/D0TC05739H

[3] B. Chen, X. Zhang, F. Wang, Accounts of Materials Research 2, 364 (2021); https://doi.org/10.1021/accountsmr.1c00041

[4] Y. Zhuang, R. Xie, Advanced Materials 33, 2005925 (2021); https://doi.org/10.1002/adma.202005925

[5] J. Yu, Q. Niu, Y. Liu, Y. Bu, H. Zou, X. Wang, Journal of Materials Chemistry C 11, 14968 (2023); https://doi.org/10.1039/D3TC02729E

[6] Z. Huang, B. Chen, B. Ren, D. Tu, Z. Wang, C. Wang, Y. Zheng, X. Li, D. Wang, Z. Ren, Advanced Science 10, 2204925 (2023); https://doi.org/10.1002/advs.202204925

[7] W. Wang, A. Tasset, I. Pyatnitskiy, H. G. Mohamed, R. Taniguchi, R. Zhou, M. Rana, P. Lin, S. L. C. Capocyan, A. Bellamkonda, W. Chase Sanders, H. Wang, Advanced Drug Delivery Reviews 186, 114343 (2022); https://doi.org/10.1016/j.addr.2022.114343

[8] W. Yang, C. Li, and L. Han, Carbon Letters (2024).

[9] A. Qasem, P. Xiong, Z. Ma, M. Peng, Z. Yang, Laser & Photonics Reviews 15, 2100276 (2021); https://doi.org/10.1002/lpor.202100276

[10] B. Chandra, V. Chandra, P. Jha, V. Sonwane, Physica B: Condensed Matter 491, 12 (2016); https://doi.org/10.1016/j.physb.2016.03.015

[11] G. Lee, S. Song, W. H. Jeong, C. Lee, J. Kim, J. Lee, J. Choi, H. Choi, Y. Kim, S. J. Lim,

Small 20, 2307089 (2024).

[12] M. A. Listyawan, H. Song, G.-T. Hwang, H.-C. Song, J. Ryu, Journal of Alloys and Compounds 923, 166250 (2022); https://doi.org/10.1016/j.jallcom.2022.166250

[13] S. Zhu, C. Song, Y. Tian, L. Ma, Materials Research Bulletin 181, 113099 (2025); https://doi.org/10.1016/j.materresbull.2024.113099

[14] Z. Monette, A. K. Kasar, P. L. Menezes, Journal of Materials Science: Materials in Electronics 30, 19675 (2019); https://doi.org/10.1007/s10854-019-02369-8

[15] K. Gi-Woo, C. Min-Young, K. Ji-Sik, Sensors and Actuators A: Physical 240, 23 (2016); https://doi.org/10.1016/j.sna.2016.01.039

[16] S. M. Jeong, S. Song, H. Seo, W. M. Choi, S. Hwang, S. G. Lee, S. K. Lim, Advanced Sustainable Systems 1, 1700126 (2017); https://doi.org/10.1002/adsu.201700126

[17] J. Cui, B. Ren, Y. Guo, S. Yang, J. Han, J. Li, Y. Cao, Measurement 241, 115693 (2025); https://doi.org/10.1016/j.measurement.2024.115693

[18] S. Mohamed, Journal of physics D: applied physics 43, 035406 (2010); https://doi.org/10.1088/0022-3727/43/3/035406

[19] A. Al-Sharabi, A. Alnehia, A.-O. Ahmed, N. A. Yahya, Albaydha University Journal 1, 224 (2019); https://doi.org/10.56807/buj.v1i2.25

[20] G.-J. Lee, S. Anandan, S. J. Masten, J. J. Wu, Industrial & Engineering Chemistry Research 53, 8766 (2014); https://doi.org/10.1021/ie500663n

[21] J. Kaur, M. Sharma, O. Pandey, Superlattices and Microstructures 77, 35 (2015); https://doi.org/10.1016/j.spmi.2014.10.032

[22] H. Ang, M. Bosman, R. Thamankar, M. F. B. Zulkifli, S. K. Yen, A. Hariharan, T. Sudhaharan, S. T. Selvan, ChemPhysChem 17, 2489 (2016); https://doi.org/10.1002/cphc.201600415

[23] M. A. Shohag, G. Adams, V. Eze, L. B. Carani, T. Ichite, O. Okoli, Journal of Luminescence 260, 119895 (2023); https://doi.org/10.1016/j.jlumin.2023.119895

[24] S. Timilsina, J. S. Kim, J. Kim, G.-W. Kim, International Journal of Precision Engineering and Manufacturing 17, 1237 (2016); https://doi.org/10.1007/s12541-016-0149-y

[25] S. Lv, Y. Han, L. Shuai, B. Chen, J. Wan, Journal of Luminescence 239, 118303 (2021); https://doi.org/10.1016/j.jlumin.2021.118303